# Microinterferometric Study of the Structure, Interfacial Potential, and Viscoelastic Properties of Polyelectrolyte Multilayer Films on a Planar Substrate

**Catherine Picart,*,†,‡ Kheya Sengupta,‡,§ Joerg Schilling,§ Gjertrud Maurstad,#,§ Guy Ladam,⊥ Andreas R. Bausch,§ and Erich Sackmann§**

*Institut National de la Santé et de la Recherche Médicale, Unité 595, Université Louis Pasteur, 11 rue Humann, F-67085 Strasbourg Cedex, France, Lehrstuhl für Biophysik, E22, Technische Universität München, James-Franck-Strasse 1, D-85748, Garching, Germany, Biophysics and Medical Technology, Department of Physics, The Norwegian University of Science and Technology (NTNU), N-7491 Trondheim, Norway, and Laboratoire de Biophysique et Biomatériaux (La2B), Université de Rouen, Centre Universitaire d'Evreux, 1 rue du 7ème Chasseurs, BP 281, F-27002 Evreux Cedex, France*

*Received: December 22, 2003; In Final Form: March 13, 2004*

Thin films of polyelectrolyte multilayers composed of alternating layers of poly(styrene sulfonate) and poly(allylamine hydrochloride) were characterized in terms of their structure, surface potential, and viscosity, by monitoring the Brownian height fluctuations of colloidal beads placed on the films using dual wavelength−reflection interference contrast microscopy (DW−RICM). Special attention was directed toward characterizing the surface properties of the probe beads. The effect of coating the beads with differently charged polymers and of having differently charged polymers as the topmost layer of the film was investigated. It was found that, unless the coated beads and the topmost layer were similarly charged, the beads were present at a lower height than expected and did not exhibit any Brownian fluctuations. In the case of well-fluctuating beads, the film thickness obtained by DW−RICM agreed well with that obtained by optical waveguide lightmode spectroscopy. The height fluctuations of the beads were analyzed to yield information about the bead/film interaction potential and the viscosity of the films. Both the viscosity and the stiffness of the potential decrease as the film thickness increases. We also report an unexpected power law dependence of the stiffness of the bead/substrate interaction potential on the height of the beads.

## Introduction

Surface modifications of materials are of primary importance for biomedical applications.[1−3] Among the different techniques used to modify surfaces, the deposition of polyelectrolyte multilayers (PEMs) has emerged as an easy to handle and versatile tool.[4−6] It involves alternate deposition of polycations and polyanions and allows the buildup of films with tunable properties by adjusting parameters such as the chemical nature of the polyelectrolytes, pH and ionic strength of the medium, and immersion and rinsing times. It is thus possible to obtain an almost infinite variety of architectures with different permeabilities,[7] optical properties,[8] or even cell adhesion properties.[9,10] One of the most investigated polyelectrolyte systems is based on poly(styrene sulfonate)/poly(allylamine hydrochloride) (PSS/PAH). These nanometer-thick multilayers have been characterized by a wide range of techniques. Both the mass and the thickness of the films have been shown to exhibit, in the dried state, a linear growth with the number of deposition steps.[11,12] PSS/PAH films were also used as a reference system for following in situ, under a liquid environment, the process of PEM buildup by various optical biosensors, such as scanning angle reflectometry (SAR),[13] optical waveguide lightmode spectroscopy (OWLS),[14,15] and a colorimetric resonant biosensor.[16] Films made of synthetic polyelectrolytes such as PSS/PAH are attracting interest as new biomaterial coatings, because they are highly biocompatible in vitro and favor the growth of primary endothelial cells and primary fibroblasts.[17,18]

For many applications, e.g., when the films are subjected to flow, deformation, shear stress, aging, or when they are used as a substrate for promoting or inhibiting cell growth,[10,17] it is important to control the mechanical properties of the film.[19]

However, the viscoelastic properties of these layer-by-layer polyelectrolyte films are still poorly understood. This is partly due to the lack of available techniques capable of probing the rheology at length scales relevant to these films whose thickness range from nanometers to micrometers. The few studies undertaken so far were focused on the elasticity and mechanical stability of hollow capsules of the polyelectrolytes.[20,21] Several techniques based on colloidal probes have recently been developed to study soft thin films. These include surface force measurements with colloidal beads attached to atomic force microscopy (AFM) tips,[22,23] total internal reflection microscopy (TIRM),[24,25] and reflection interference contrast microscopy (RICM).[26−28]

Using conventional RICM, it is possible to measure the instantaneous height (i.e., the distance from the underlaying substrate) of colloidal beads hovering over transparent planar substrates in a liquid medium and to reconstruct the bead/surface interaction potentials from the height distribution functions. As in any interferometric technique using monochromatic light, the

* Author to whom correspondence should be addressed. Telephone: 33-3-90-24-32-58. Fax: 33-3-90-24-33-99. E-mail: Catherine.Picart@medecine.u-strasbg.fr.

† Université Louis Pasteur.

‡ Authors C.P. and K.S. contributed equally to the work.

§ Technische Universität München.

# NTNU.

⊥ Université de Rouen, Centre Universitaire d'Evreux.

10.1021/jp037971w CCC: $27.50 
Published on Web 04/30/2004

height determination has an inherent ambiguity of approximately half the wavelength of the light used, which is usually of the order of 200 nm. Recently, the RICM technique was further modified to include a second wavelength (dual wavelength, or DW−RICM), which enables the measurement of absolute heights up to ∼800 nm with an accuracy of 3 nm.[29] With this technique, the interaction potentials and the effective surface friction coefficients can be measured as a function of the absolute distances of the beads from the substrate. DW−RICM is thus ideal for investigating the surface properties of thin nanostructured films. However, in all the techniques involving colloidal probes, including DW−RICM, it is important to first characterize the probe beads, in terms of their surface properties, because the bead surfaces are typically not smooth and hard but exhibit some roughness, fuzziness, and hairiness, as a result of the polymer nature of polystyrene, which is the material that typically comprises colloidal beads.[30,31]

In this paper, we report the characterization of thin films made of PEMs, in terms of their thickness, surface potentials, and surface friction coefficients using DW−RICM, with special attention to the influence of bead/film interaction on the measured parameters. The beads to be used as probes were first characterized in terms of the fuzziness of their surface. Next, the DW−RICM technique was validated for absolute height measurements by comparing the heights of multilayer films of controlled thickness, as measured by DW−RICM, with OWLS data. The influence of having different coatings on the beads and of different polyelectrolytes (PSS or PAH) as the topmost layer on the behavior of the beads was investigated. Finally, the bead/film interaction potential and the surface friction coefficient of the films was obtained by monitoring the thermal fluctuations of colloidal beads placed on the films. The interaction potential was characterized by its double derivative (i.e., the curvature) at the minimum (i.e., around the equilibrium height) and was compared to previous studies of colloidal beads on glass substrates and on hyaluronic acid cushions.[27,28] An unexpected universal power law dependence of the curvature of the interaction potential on the bead height is reported.

## Materials and Methods

**Substrates.** Glass slides (24 mm × 24 mm, VWR Scientific) that were cleaned by sonication in a 2% v/v detergent solution (Hellmanex, Hellma, Germany), followed by repeated washing and sonication in ultrapure water (Milli Q-Plus system, Millipore, Bedford, MA), were used as bare glass substrates. Similar slides that were cleaned with 10 mM sodium dodecyl sulfate (SDS) and 0.1 N HCl and extensively rinsed with pure deionized water were used as substrates for the polyelectrolyte multilayers.

**Polyelectrolyte Solutions.** Poly(sodium 4-styrene sulfonate) (PSS, 70 kDa), poly(allylamine hydrochloride) (PAH, 70 kDa), and poly(ethyleneimine) (PEI, 700 kDa) were purchased from Sigma−Aldrich. All solutions were prepared using ultrapure water (Milli Q-Plus system, Millipore) with a resistivity of 18.2 MΩ cm. Polyelectrolyte solutions were prepared by direct dissolution in a filtered 0.15 M NaCl solution at pH 6 in order to have a final concentration of 5 mg/mL.

**Beads.** Carboxyl-modified polystyrene beads with a diameter of 10.15 ± 0.06 $\mu$m were purchased from Duke Scientific (Palo Alto, CA). For experiments on glass, the beads were used after washing in ultrapure water. For experiments on PEM films, beads were coated with bovine serum albumin (BSA) (Sigma−Aldrich, incubation for 30 min), followed by three rinsing steps. Beads were also coated with PSS or PAH following the same procedure. Sulfate-modified polystyrene beads with a diameter of 9.6 ± 0.7 $\mu$m were purchased from Interfacial Dynamics Corporation (Molecular Probes, Eugene, OR). Prior to use, the beads were washed with ultrapure water.

Experiments on bare glass with Duke and IDC beads were performed in potassium chloride (KCl) solutions of various ionic strengths.

**Automatic Buildup of the Polyelectrolyte Multilayered Films.** In the following, films ending with a PAH (positive) layer are called PEI−(PSS/PAH)$_i$ films and films ending with a PSS (negative) layer are called PEI−(PSS/PAH)$_i$−PSS. The subscript "*i*" refers to the number of PSS/PAH layer pairs.

All the PEI−(PSS/PAH)$_i$ films were prepared with an automatic dipping machine (Dipping Robot DR3, Kirstein GmbH, Germany). First, a precursor layer of PEI was deposited on the glass substrates. The glass slides were arranged vertically in a homemade holder that was immersed for 10 min in a first polyelectrolyte solution (PEI). The slides were subsequently rinsed successively in three different beakers, containing 0.15 M NaCl solution (pH 6), of volumes of 350, 200, and 200 mL for 2, 6, and 6 min, respectively. They were then dipped into the oppositely charged polyelectrolyte solution (PSS) followed by the same rinsing procedure. The entire procedure was repeated with the PAH solution and so on. Rinsing solutions were changed after the deposition of every tenth layer. Slides were stored in 6-wells culture plates at 4 °C.

**Analysis of Film Growth and Zeta Potential.** The PEI−(PSS/PAH)$_i$ film buildup process was followed in situ by OWLS.[32,33] Briefly, OWLS is sensitive to the penetration depth of an evanescent wave (∼200−300 nm) traveling through a polymer film deposited on a waveguide surface and gives access to the optical properties of the film. The effective refractive indexes of the waveguide—NTE and NTM for the transverse electric and transverse magnetic waves, respectively—are measured. From these, the film refractive index ($n_A$) and thickness ($d_A$) can be deduced by solving the phase equations. This method has already been experimentally applied to polyelectrolyte multilayers.[15,34] One hundred microliters of the polyelectrolyte solutions was injected (alternately polycation and polyanion), left at rest for 15 min, and rinsed under constant flow (rate 7 mL/h) for 12 min with the NaCl solution.

The zeta potential of the layers adsorbed on a capillary were measured using a homemade streaming potential measurement apparatus.[35] The apparatus and the experimental procedure have been previously described.[13,36] The adsorption of PSS and PAH was performed in a 0.15 M NaCl solution, and measurements were performed after a rinsing step, following the deposition of each layer. The rinsing solution (also present during the measurements) contained only 0.5 mM Tris at pH 6.

**Dual-Wavelength Reflection Interference Contrast Microscopy (DW−RICM) Technique.** The DW−RICM technique has been described in detail elsewhere.[29] In conventional RICM, monochromatic light is incident on the bead under study, which typically hovers over a bare glass substrate or a transparent polymer film (deposited on a glass substrate) in a liquid medium. The incident light is reflected from the glass/buffer interface and again from the buffer/bead interface. These two reflected rays interfere and result in the characteristic RICM interference pattern that consists of concentric dark and bright circular fringes in case of spherically symmetric objects such as beads. The major drawback of the conventional RICM technique is that the information about the absolute phases of the beams reflected by the various interfaces of a film is not known. Therefore, absolute distances cannot be measured, because there is an ambiguity of a factor $\lambda/(2n)$ (where $\lambda$ is the

wavelength of the light used and $n$ is the refractive index of the medium). This drawback can be overcome by comparing the interferograms obtained simultaneously with two different wavelengths. In other words, an additional periodicity and boundary condition is introduced by observing a second wavelength. This enables the measurement of absolute heights of the beads above a planar surface.

A reflection interference contrast inverted microscope (Axiomat Zeiss, Germany) that was equipped with an antiflex objective (63×, oil immersion, N.A. = 1.3) was used. In this setup, the sample is illuminated through the objective by a bichromatic light beam ($\lambda$ = 546 and 436 nm) generated by passing the light from a 100 W mercury vapor lamp (Osram, Germany) through an interference filter (IF filter, 85% transmission, 12 nm waveband; AF-Analyzetechnik, Germany). Just before recording the image, the images corresponding to the two wavelengths are separated by a dichroic mirror and recorded with two charge-coupled device (CCD) cameras (models 4880-85 (10 bit) and 4742-95 (12 bit), Hamamatsu, Japan).

The heights of the beads were determined, within the $\lambda/(2n)$ ambiguity, from the radii of the interference fringes obtained using $\lambda$ = 546 nm. In principle, for a bead of radius $R$, the height $h(r_l)$ and the radius of the $l$th fringe $r_l$ are related by

$$h(r_l) = \frac{\lambda}{2n} - R + \sqrt{R^2 - r_l^2}$$

However, in this equation, the curvature of the bead has not been taken into account. Therefore, a more accurate empirical relation[29] was used to determine the heights of the beads. The ambiguity of $\lambda/(2n)$ in the height was removed by comparing the interferograms obtained with the two wavelengths. Using this technique, the absolute and relative heights of a bead can be determined respectively with an accuracy of ~3 nm about ~0.4 nm.

**Determination of the Interfacial Potential and the Surface Viscosity.** The Brownian motion of a colloidal bead in an interfacial potential $V(h)$ can be described by the Langevin equation:

$$m\frac{\partial^2 h}{\partial t^2} + \gamma\frac{\partial h}{\partial t} + \frac{\partial V}{\partial h} = f_{\text{stoch}} \qquad (1)$$

where $h$ is the distance of the bead from the substrate, $m$ the mass of the bead, $t$ the time variable, and $f_{\text{stoch}}$ the stochastic force due to thermal noise. In the case of a colloidal bead, the inertial term (the first term on the left-hand side) can be neglected. The second term accounts for the viscous force, where $\gamma$ is an effective friction coefficient. The third term accounts for the interfacial interaction potential $V(h)$ between the bead and the polymer film. For small deformations, $V(h)$ can be expressed in terms of a harmonic potential $V(h) = V''(\Delta h)^2$, where $V'' = \partial^2 V/\partial h^2$ and $\Delta h = h - \langle h\rangle$. $V''$ is a measure of the stiffness of the interfacial potential.

The effective friction $\gamma$ experienced by a sphere exhibiting steady-state motion at a distance $h$ from a wall is determined by a modified Stoke's law:[37,38]

$$\gamma = 6\pi R\eta_{\text{eff}} F\left(\frac{R}{h}\right) \qquad (2)$$

where the function $F(R/h)$ accounts for the fluid drainage between the bead and the wall and $\eta_{\text{eff}}$ is the effective surface viscosity.

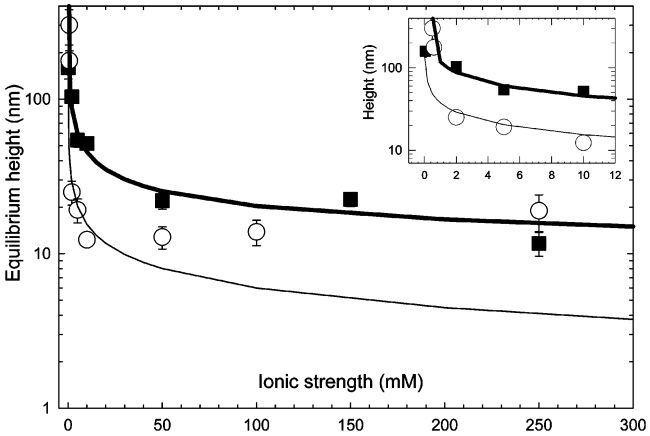


**Figure 1.** Experimental and theoretical equilibrium heights as a function of the ionic strength for two different types of beads hovering over a bare glass substrate. Experimental points were determined by the dual-wavelength-reflectance interference contrast microscopy (DW−RICM) technique (■) for carboxyl-modified beads from Duke and (○) for sulfate-modified beads from IDC. The lines correspond to the theoretical equilibrium heights calculated using eq 6 with the surface charge of the glass substrate given as $\sigma_G$ = 0.0007 C/m$^2$. The thin solid line corresponds to IDC beads ($\sigma_B$ = 0.0001 mC/m$^2$, no fuzzy layer), and the thick solid line corresponds to Duke beads ($\sigma_B$ = 0.0005 C/m$^2$, fuzzy layer of 7 nm). Inset shows an enlarged view of the low ionic strength range (0−12 mM).

The two viscoelastic parameters $V''$ and $\gamma$ can be determined by calculating the time correlation function of the fluctuation of the distance between the bead and the substrate, according to

$$\langle h(t)h(t+\tau)\rangle = \frac{k_B T}{V}\exp\left(\frac{-V''}{\gamma}\tau\right) \qquad (3)$$

The interaction potential can also be obtained from the probability distribution of the heights using Boltzmann's law:[26]

$$V(h) = -k_B T \ln\left(\frac{P(h)}{P_0}\right) \qquad (4)$$

For our measurements, we have confirmed that both methods yield approximately the same value for $V''(h)$ (data not shown).

## Results and Discussion

**Characterization of Probe Beads.** The absolute equilibrium height of colloidal beads hovering over glass substrates were measured as a function of the ionic strength of the medium, which was varied from 0.5 mM to 0.3 M by adding KCl. Measurements were performed with carboxyl-modified (Duke) and sulfate-modified (IDC) beads.

In Figure 1, the measured equilibrium heights of the beads are plotted against the ionic strength of the buffer. Each data point corresponds to the average equilibrium height calculated from at least five different beads; the error bars indicate the standard deviations of the distributions.

The interfacial interaction potential experienced by the beads is expected to be the sum of three contributions: the electrostatic double layer repulsion, gravity, and the van der Waals force. When the separation distance is greater than several Debye lengths, the van der Waals attraction is expected to be severely retarded and screened[24] and can, therefore, be neglected. Also, the double-layer repulsion is expected to be well-modeled using

linear superposition and Derjaguin's approximation. This interaction potential is given by

$$V(h) = B\exp(-\kappa h) + Ch \tag{5}$$

where

$$B = 4\pi R\epsilon_0\epsilon_R\left(\frac{kT}{e}\right)^2 \tanh\left(\frac{e\psi_B}{4kT}\right)\tanh\left(\frac{e\psi_G}{4kT}\right)$$

and

$$C = \frac{4}{3}\pi R^3(\rho_B - \rho_F)g$$

$\epsilon_0$ and $\epsilon_R$ are, respectively, the permittivity and relative dielectric constant of water, $R$ is the radius of the sphere, $e$ is the elemental charge, and $\psi_B$ and $\psi_G$ are the Stern potentials of the bead and the glass wall. The reciprocal screening length is given as

$$\kappa = \sqrt{\frac{8\pi Ie^2}{\epsilon k_B T}}$$

where $I$ the total ionic strength, $k_B$ the Bolzmann constant, and $\rho_B$ and $\rho_F$ are the densities of the bead and the medium, respectively. The surface potentials (of both glass (G) and polystyrene bead (B)) are related to the surface charge densities ($\sigma_B$) by the Graham equation:[39]

$$4\pi\lambda_B\sigma_G = -2\kappa\sinh\left(\frac{\psi_G}{2}\right)$$

with

$$\lambda_B = \frac{e^2}{4\pi\epsilon_0 kT\epsilon_R}$$

Equation 5 can then be minimized to obtain the theoretically expected equilibrium height ($h_{EQ}$), given by

$$\kappa h_{EQ} = \ln\left(\frac{\kappa B}{C}\right) \tag{6}$$

Contrary to expectations from theoretical consideration, heights of ~20 nm were measured for the carboxyl-modified Duke beads at high salt concentrations (≥50 mM). At these ionic strengths, the Coulomb repulsion is expected to be screened and the beads are expected to "salt out" or sediment out of solution, onto the substrate. However, when the beads were placed on a positively charged surface (glass slides coated with aminosilane), the measured height was of the order of a few nanometers. It was also possible to push the beads closer to a bare glass surface by applying an external downward mechanical force. All these observations are consistent with the hypothesis that a fuzzy polymer layer is present around the bead,[31,40] and this layer is too dilute to reflect light but nevertheless marks the mechanical boundary of the particle. When an external force is applied, either in the form of Coulomb attraction from a positively charged surface or as a downward mechanical force, the dilute fuzzy layer gets compressed and the bead is driven closer to the substrate. The thickness of this fuzzy layer depends strongly on the surface modification of the bead and can vary, even for the same chemical surface modification, from one manufacturer to the other (data not shown). Thus, in experiments using optical techniques that necessarily rely on the optical density of the bead, the bead appears to be higher than it really is, because of the presence of the fuzzy layer.

For fitting the experimental heights shown in Figure 1 with eq 6, the surface charge of the glass substrate was taken to be $\sigma_G = 0.0007$ C/m$^2$, according to von Grünberg.[41] The only free parameter in the fitting was the surface charge density of the bead, which was varied in order to optimize the fit. It was found that the measured heights were always consistently higher than the expected height. However, adding a constant height $h_{fuzz}$ to the $h_{EQ}$ value, to account for the fuzzy layer, improves the fit significantly (the thick solid line in Figure 1). The best values for $h_{fuzz}$ and the bead surface charge density ($\sigma_B$) were determined to be 7 nm and 0.0005 C/m$^2$, respectively. The fuzzy layer thickness estimated here is approximately the same as the surface roughness estimated from AFM observations.[24]

The second type of beads (IDC) considered were sulfate-modified polystyrene. The theoretical equilibrium height curve is plotted as a thin solid line in Figure 1 (with $h_{fuzz} = 0$ and $\sigma_B = 0.0001$ mC/m$^2$) and fits the data adequately for concentrations of <50 mM. The best fit for the fuzzy layer thickness was zero. Contrary to expectations, the height of the IDC beads increases at high salt concentrations. We believe that these deviations are unlikely to result from zeta potential effects, because the zeta potential shift toward more-positive values (in the case of our beads, which have large negative charges, the charge should become less negative, that is, shift toward zero charge) when the ionic strength is increased, thus leading to an enhanced attraction (or reduced repulsion) between the bead and the glass substrate. On the other hand, the RICM interference fringes indicate that, above an ionic strength of 50 mM, the average bead size increases with the salt concentration, which, in turn, leads to a decrease in the bead density. The increase of height with salt concentration is thus attributed to the decrease in bead density.

It is also possible to extract from the height fluctuations the interfacial interaction potential experienced by the beads. The potential energy of Duke beads hovering over bare glass in media of different ionic strengths is shown in Figure 2. The data points are represented by symbols and the expected theoretical potentials (calculated from eq 5) are represented as solid lines. As can be seen, the theoretical curve agrees well with the data for low ionic strengths (up to ~10 mM). At ionic strengths of 5 mM and above, the observed potentials are more symmetric than expected, because the slope $C$ of the attractive portion of the measured potential is higher than that expected from gravity alone. The discrepancy between theory and experiment becomes larger as the ionic strength increases (corresponding to lower heights), and, at 50 mM or more, the theoretical and experimental curves are totally mismatched.

In the second part of this work, measurements were performed on PEMs using the monodisperse Duke beads as probes. Because the size of each bead can be determined from the RICM interference fringes, IDC beads could, in principle, also be used. However, beads of different sizes have different weights and, hence, compress the films differently. Therefore, although the Duke beads exhibit a fuzzy layer, they were preferred over the IDC beads, because they are more monodisperse.

**Growth of PSS/PAH Films.** As a first check of the growth of the PSS/PAH films, we used the well-established in situ OWLS technique. A typical curve obtained during the successive adsorption of PSS and PAH from 0.15 M NaCl solutions is shown in Figure 3. The increase in the effective refractive index NTM (raw signal) after the addition of each new layer indicates polyelectrolyte adsorption. The charge overcompensation that

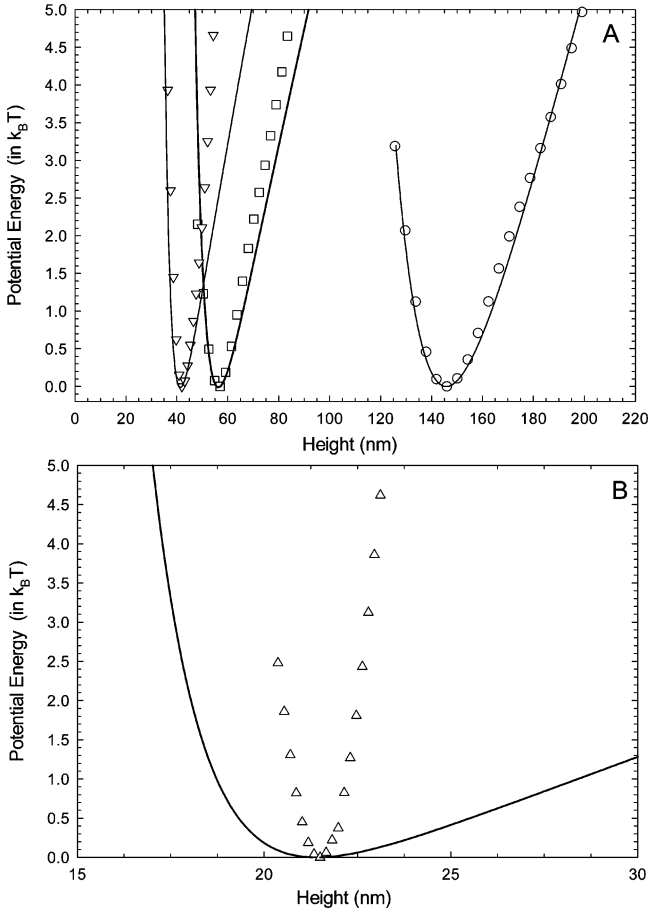


**Figure 2.** Experimental potential energy profiles determined from the height fluctuations of the beads for 10-$\mu$m polystyrene spheres interacting with a bare glass slide at various ionic strengths: (A) (○) 0.5 mM, (□) 5 mM, and (▽) 10 mM, and (B) (△) 50 mM. Each curve corresponds to one single bead. Solid curves are calculated from eq 5, using $\rho_B - \rho_F = 100$ and $R = 5.2$ $\mu$m. Changing the ionic strength changes the slope of the right-hand side of the theoretical profiles but only slightly. The slope is given by $C$, which depends on $\rho_B - \rho_F$, and $R$ is the radius of the sphere.

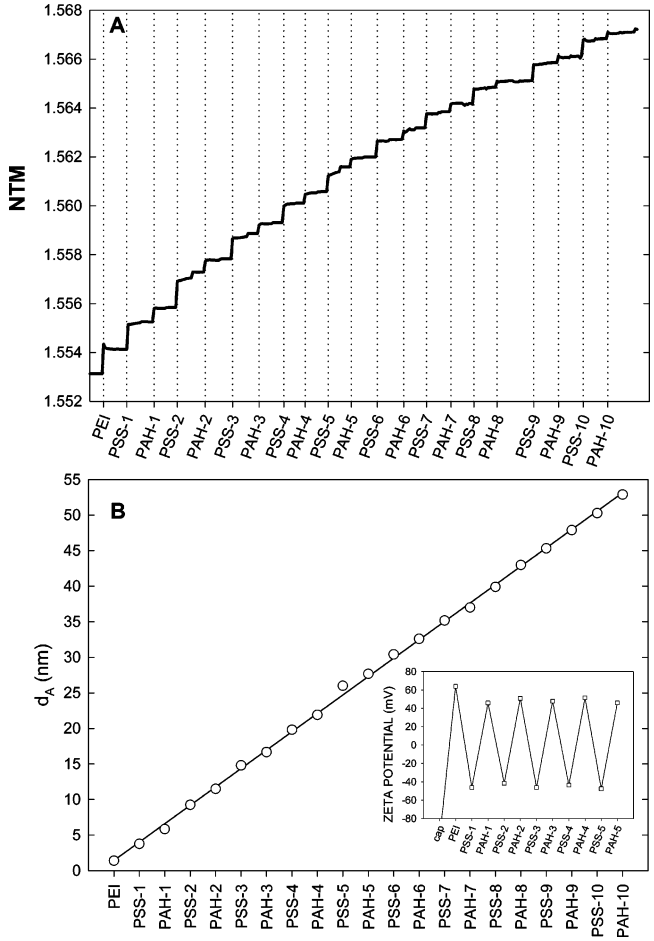


**Figure 3.** (A) Raw NTM signal obtained as a function of time during a PEI−$(PSS/PAH)_{10}$ film buildup from a 0.15 M NaCl solution, as measured by the optical waveguide lightmode spectroscopy (OWLS) technique. Dotted lines indicate the polyelectrolyte injection steps. (B) Thickness obtained by OWLS as a function of the number of layers. Inset shows the evolution of the zeta potential of a PEI−$(PSS/PAH)_5$ film during its buildup. A linear fit was added to guide the eyes.

appears on the surface after each deposition constitutes the driving force for the deposition of the next layer. The zeta potential of these films alternated between negative and positive values. It was approximately −50 mV for PSS-ending layers and approximately +55 mV for PAH-ending layers (see inset in Figure 3). The thickness increased linearly with the number of bilayers, and after the deposition of 10 layer pairs, the mean thickness estimated by OWLS was determined to be ∼50 nm with a film refractive index of $n_A = 1.5$.

**BSA Beads on PSS-Ending Films: Film Thickness and Interaction Potential.** The validity of the DW−RICM technique for thickness measurements of thin PEM films was checked with PSS/PAH multilayers of various well-controlled thicknesses. BSA-coated beads are known to be passivated, with respect to hydrophobic attraction,[42] and PSS is known to interact only slightly with albumin.[43] Therefore, in the first set of experiments, PSS-ending films were studied using BSA-coated beads as colloidal probes.

PEI−$(PSS/PAH)_i$−PSS films with the number of layer pairs "$i$" in the range of 5−30 were studied**.** The absolute equilibrium heights of the beads are plotted in Figure 4A for all the PSS-ending films. Each data point is obtained by averaging the heights of at least 16 beads on at least 2 different samples. The error bars correspond to the standard deviation of the heights obtained for a given number of layer pairs. The absolute height of the beads, as well as the inhomogeneity in the bead height distribution, increase as the number of layer pairs increases; the highest scatter in the height data is observed for 30 layer pairs (where the height ranges from 80 nm up to 260 nm). The dotted line in Figure 4A is the regression line obtained from OWLS data from films up to 10 layer pairs, which was linearly extrapolated to 30 pairs of layers. The experimental height of the beads obtained by RICM matches the extrapolated thickness from OWLS data fairly well. A slight deviation is observed for the thinnest films comprising 5 layer pairs. This discrepancy may be related to the fact that, even on bare glass, bare beads at 150 mM NaCl exhibited an average height of ∼20 nm (see Figure 1). The error bars reflect the heterogeneity of both the PEM film and the bead surface. The standard deviation of the height fluctuations of the beads is represented versus the number of layer pairs in Figure 4B. As the number of layer pairs increases, the height fluctuations are larger and more disperse. For films containing more than 30 layer pairs, the interference patterns were highly distorted, especially for the weaker blue light, because of the high layer thickness combined with a rather high refractive index (1.5) of the polyelectolyte film (Figure 5). As a consequence, images from films containing more than 30 layer pairs could not be analyzed.

PEM films are rather soft; therefore, the relatively large colloidal beads used here compress and/or sink into the film,

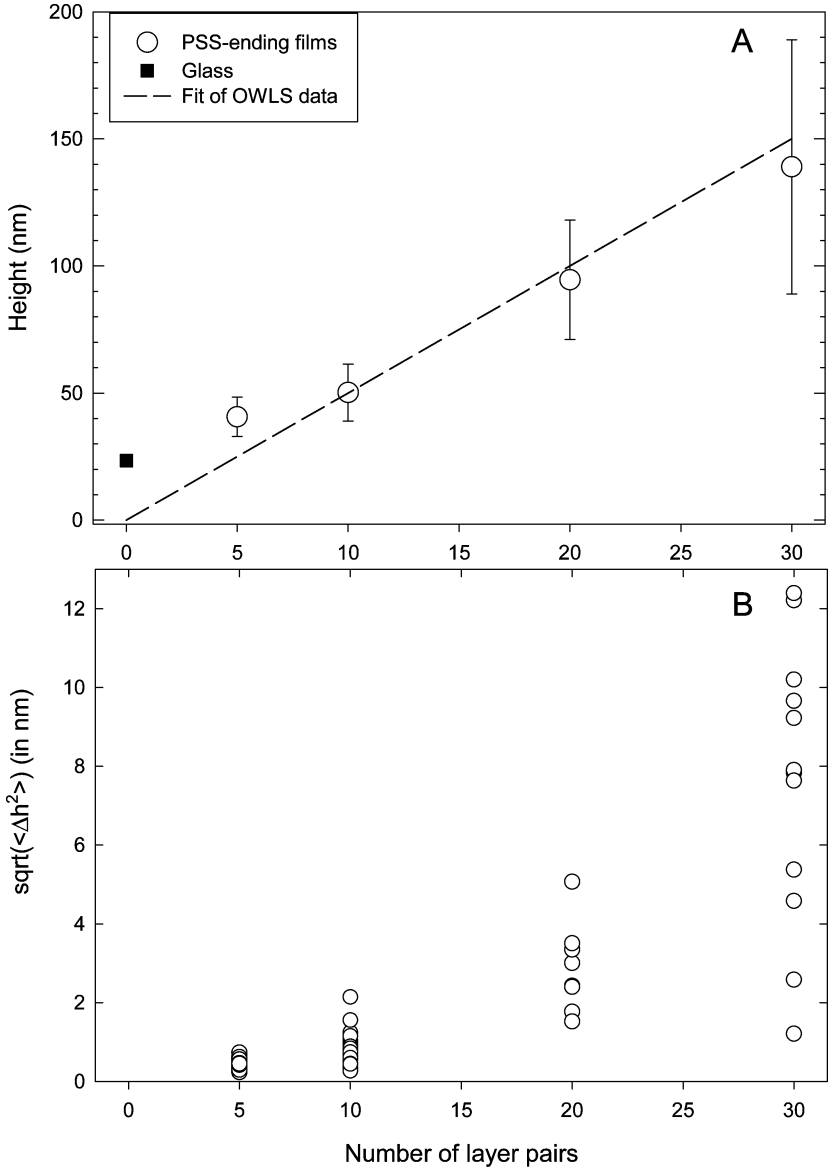


**Figure 4.** (A) Absolute height of BSA-coated beads on the PEI−(PSS/PAH)$_i$−PSS multilayer films, as measured by the DW−RICM technique, as a function of the number of layer pairs ($i$ = 5, 10, 20, 30). Symbols represent averages over all the beads for a given number of layer pairs. The error bars represent the dispersion in the height data. (B) Standard deviations of the height fluctuation of the beads as a function of the number $i$ of layer pairs in the film. Each symbol corresponds to one bead and represents the amplitude of fluctuation.

which leads to a decrease in the apparent thickness of the film. On the other hand, because of the fuzzy layer around the bead, the bead appears to be slightly higher than it is in reality, thus increasing the apparent thickness of the film. Moreover, in the height calculations, we have not taken into account the fact that the refractive index of the polymer films ($n_F$) is higher than that of water ($n$), the medium for which the beads were calibrated. This leads to two effects. The first effect results from the fact that the optical path traveled by the ray that gets reflected from the bead now travels through a medium with a refractive index of $n_F = 1.500$, instead of through water that contains salt, with a refractive index of $n = 1.334$. This leads to an increase in the path difference between the two reflected rays and, therefore, an increase in the apparent height by a factor of $n_F/n \approx 1.12$. The second effect is more subtle and results from the fact that the radii of the interference fringes and, hence, the calculated heights depend on the refractive index of the film.

For the PSS/PAH films studied here, these three effects—namely, film compression, steric levitation (the fuzzy layer effect), and the refractive index effects—compensate each other in such a way that the measured data remain close to the line extrapolated from OWLS data. The interaction potential of the beads on PSS/PAH films of various thicknesses are represented in Figure 6 (note the difference in scale of the abscissa between panels A and B). A comparison with Figure 2 shows that the potentials over the PEI−(PSS/PAH)$_i$−PSS films are different from the potentials over glass at an equivalent ionic strength. The stiffness of the potential decreases as the number of layers increases.

**PSS- or PAH-Coated Beads on PSS-Ending Films: Influence of Bead Coating.** The effect of coating the beads with different polymers (PSS or PAH) on the bead/film interaction potential was explored. Duke beads were coated either with PSS or with PAH and were placed on PSS-ending PEM films. As a polycation, PAH adsorbs onto polystyrene[10] and also onto carboxyl-modified surfaces groups, because of its positive charge. In case of PSS, the adsorption is not because of the charge but because of hydrophobic interactions with the modified polystyrene beads.[42]

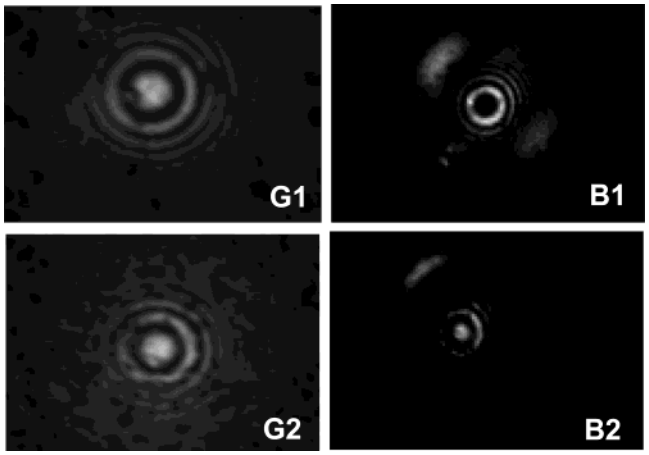


**Figure 5.** DW−RICM interference patterns obtained using two wavelengths (**G** denotes green at 546 nm and **B** denotes blue at 436 nm) for two 10-$\mu$m beads hovering over PSS-ending films made of 30 layer pairs (**G1** and **B1**) and 50 layer pairs (**G2** and **B2**). For the 50 layer pairs, the interference pattern is highly distorted and, therefore, is not amenable to further analysis.

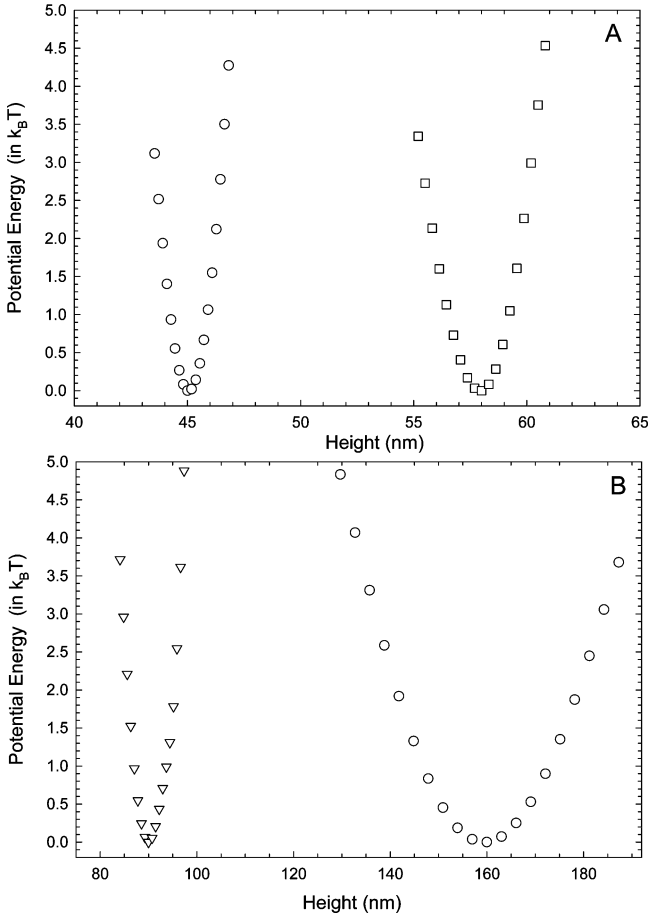


**Figure 6.** Potential energy profiles for 10-$\mu$m polystyrene spheres hovering over PEI−(PSS/PAH)$_i$−PSS multilayer films made of an increasing number of bilayers ($i$ = 5, 10, 20, 30) in a 0.15 M NaCl solution (pH 6.5): (A) (○) $i$ = 5 and (□) $i$ = 11; (B) (▽) $i$ = 20 and (○) $i$ = 30. (Note the difference in the height scale for the two graphs.)

As a control, the behavior of the coated beads on bare glass (buffer ionic strength 0.15 M NaCl, pH 6.5) was checked. The average height of the BSA-coated beads (22.5 ± 2.3 nm) was similar to that of the PSS-coated beads (21.9 ± 5.5 nm); however, the dispersion in the measured heights was higher for the PSS-coated beads. The height fluctuations of the BSA- and

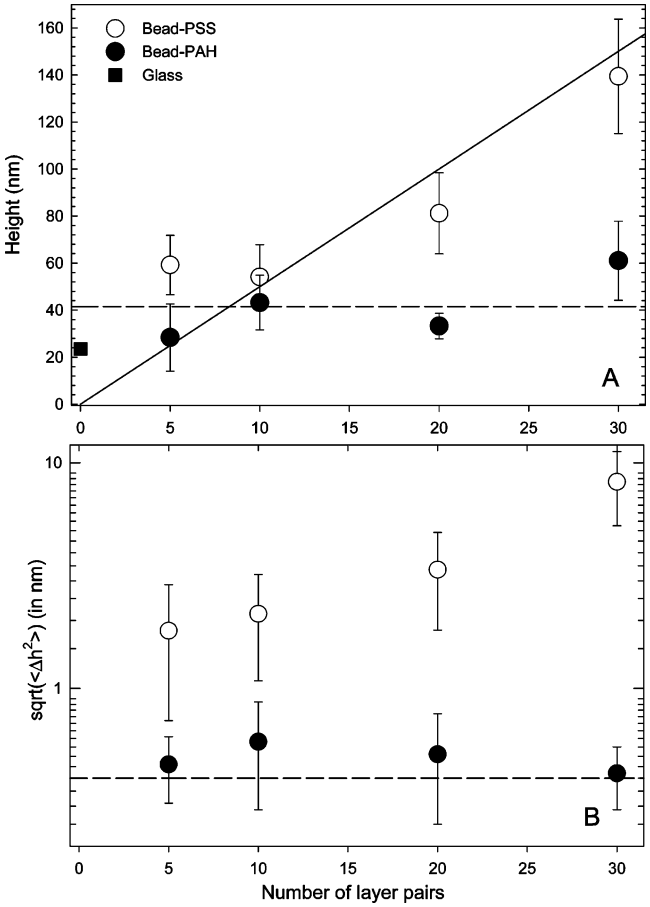


**Figure 7.** (A) Absolute heights of the PEI−(PSS/PAH)$_i$−PSS multilayer films, as measured by the DW−RICM technique, as a function of the number of bilayers $i$ for (○) PSS-coated beads and (●) PAH-coated beads. The solid line represents the fit obtained with OWLS data, and the dashed line represents a line of height 42 nm, which is the average of all the heights measured on the PAH-ending samples. (B) Standard deviations of the height fluctuations for all the beads, as a function of the number of layer pairs $i$ in the PEM film (with same symbols as for panel A). Each symbol is the mean of all the data obtained for at least 16 beads on two different PEM films (of same $i$) with the corresponding standard deviation. Dashed line corresponds to fluctuations of 0.4 nm, which is the experimental limit of resolution.

PSS-coated beads with standard deviations of 0.5 ± 0.3 nm and 0.4 ± 0.3 nm, respectively, were also similar. The positively charged PAH-coated beads were slightly lower (17.9 ± 2.2 nm), indicating an attractive interaction of the beads toward the glass substrate. Free PAH molecules from a solution are known to adsorb onto a bare glass substrate.[44] Therefore, it can be conjectured that, in the present case, the PAH molecules that are adsorbed onto the bead surface facilitate its attraction to the glass substrate.

The behavior of the coated beads placed on the PEM films ending with a PSS layer depends crucially on the nature of the bead coating. The most obvious difference is that, whereas the PSS-coated beads fluctuate in a manner similar to that of BSA-coated beads on similar films, the PAH-coated beads do not experience any fluctuation whatsoever.

The absolute heights of the beads with the two different polymer coatings, as a function of the number of pairs of layers in the film, are shown in Figure 7. A comparison with Figure 4 shows that the measured heights for the PSS-coated beads are very close to that of the BSA-coated beads. The height fluctuations are consistently larger for the PSS-coated beads (Figure 7B) than for the BSA-coated ones (Figure 4B). This is

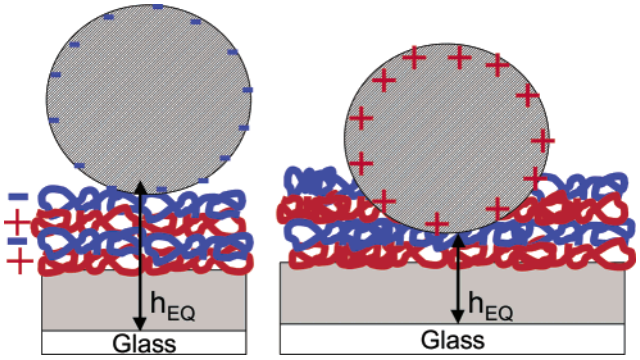


**Figure 8.** Scheme of the interaction of a colloidal probe with a PSS/PAH multilayer film (PSS being the polyanion and PAH the polycation) on top of a PSS-ending film for a BSA- or PSS-coated bead and for a PAH-coated bead. For clarity, only a few bilayers have been represented; the gray zone represents many bilayers. The parameter $h_{EQ}$ is the equilibrium height of the bead measured by DW−RICM. In the left panel, the bead is hovering over the film, whereas in the right panel, it is stuck into the film.

**TABLE 1: Averages and Standard Deviations of the Height Fluctuations of the Beads on Top of PEI−(PSS/PAH)$_i$−PAH-Ending Films[a]**

| number of layer pairs, $i$ | Bead Coating (nm) | | |
|---|---|---|---|
| | BSA | PSS | PAH |
| 5 | 0.6 ± 0.5 (20) | 0.4 ± 0.2 (10) | 0.7 ± 0.5 (17) |
| 10 | 0.7 ± 0.5 (12) | 0.8 ± 0.7 (12) | 1.0 ± 0.7 (12) |
| 20 | 0.6 ± 0.5 (10) | 0.5 ± 0.2 (11) | 1.7 ± 0.7 (10) |
| 30 | 0.5 ± 0.3 (9) | 0.7 ± 0.6 (10) | 1.1 ± 0.4 (10) |

[a] Beads were coated with BSA, PSS (negative), or PAH (positive). The number of beads over which an average was obtained is given in parentheses.

likely to be a consequence of the steric and Coulomb repulsive interactions between the PSS coating of the beads and the PSS outer layer of the film.

In case of PAH-coated beads, the bead heights and, hence, the apparent film thickness did not increase with the number of layers (Figure 7A) but remained approximately constant at ∼42 nm. The maximum height measured was ∼60 nm. The amplitude of the height fluctuation is ∼0.4 nm, which is close to the limit of resolution of the experiment (Figure 7B).

The low bead heights and low amplitude of height fluctuations of the PAH-coated beads suggest that these beads get embedded into the PEM film. A possible mechanism could be a step-by-step bead/PEM interaction, such that the positively charged PAH coating of the bead first interacts with the negatively charged outermost PSS layer of the film. At this stage, the bead gets partially covered with negatively charged PSS, which then interacts with the next underlying positively charged PAH layer, and so on. In the case of negatively charged PSS-covered beads, the similarly charged PSS on the outermost layer of the PEM film has a repulsive interaction with the bead, preventing it from undergoing further interaction with the underlying layers. Figure 8 summarizes why PSS- or BSA-coated beads do not sink into the film, whereas PAH-coated beads do.

**Experiments on PAH-Ending Films.** In the next set of experiments, the behavior of the coated beads on PAH-ending PEM films was studied. The BSA- and PSS-coated beads were at a height of ∼50 nm, irrespective of the number of layers in the PEM films, and did not exhibit any height fluctuations (see Table 1). Since BSA- and PSS-coated beads are negatively charged, they are expected to experience an attractive interaction with the positively charged PAH-ending films. Moreover, it has been demonstrated by SAR that albumin adsorbs strongly onto

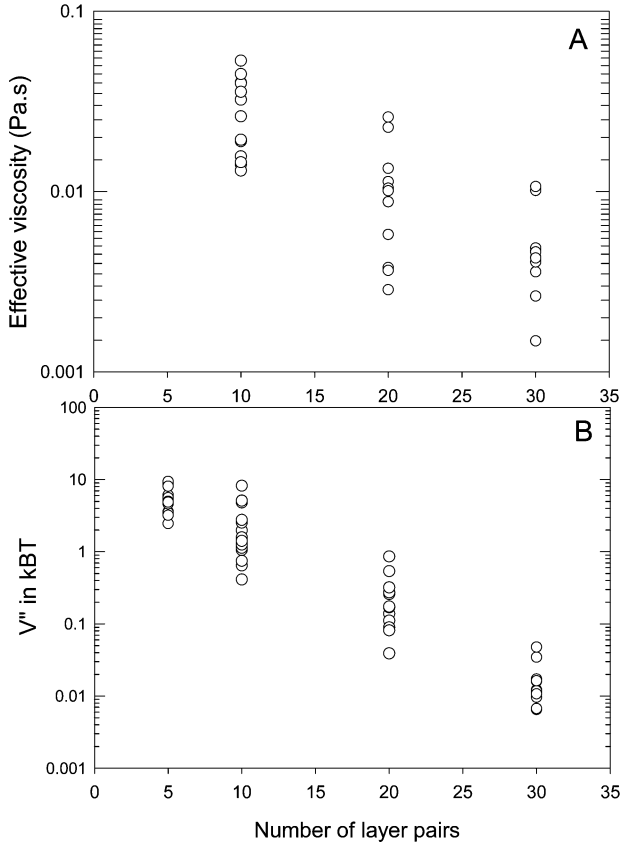


**Figure 9.** (A) Effective surface viscosity as a function of the number of layer pairs $i$ in the film for the same beads, and (B) evolution of the second derivative of the interaction potential $V''$ (force constant characterizing resistance of the film against elastic deformation), as a function of the number of layer pairs $i$ in the PEI−(PSS/PAH)$_i$−PSS films for BSA-coated Duke beads.

PAH-ending films but only weakly on PSS-ending films.[43,45] Therefore, the absence of fluctuations and the uniform bead height for all the samples can again be attributed to the attractive interaction of the beads with the positively charged outermost layer of the films, eventually leading to the beads getting embedded in the films (Figure 8).

Unexpectedly, PAH-coated beads on PAH-ending films did not exhibit significant height fluctuations. This may originate from an imperfect coating of the beads with PAH and/or the presence of defects in the positive topmost layer, which expose the negative layers underneath and lead to attractive bead/film interactions.

**Film Viscosity and Bead/Film Interaction Potential.** The effective friction—and, hence, the effective surface viscosity ($\eta_{eff}$)—experienced by a bead can be calculated from the height correlation function, using eqs 3 and 4. When, as in the present case, the bead fluctuates near a hard wall (the glass substrate) with $R \gg h$, $F(R/h)$ in eq 2 can be approximated as $F(R/h) \approx R/h$.[46] Because the bead is only partially submerged in the polyelectrolyte film, the effective viscosity has contributions from both the surrounding buffer and the film. Note that the viscosity reported here is a sum of these two contributions and characterizes the entire film/buffer interface. In Figure 9A, $\eta_{eff}$ (for BSA-coated beads on PSS-ending films) is plotted as a function of the number of layer pairs in the PEM film. As can be seen, $\eta_{eff}$ decreases as the number of layer pairs increases. For a 50-nm-thick film made of 10 layer pairs, the effective viscosity is ∼10 times that of water, whereas a film containing 30 layer pairs is only four times more viscous than water. This

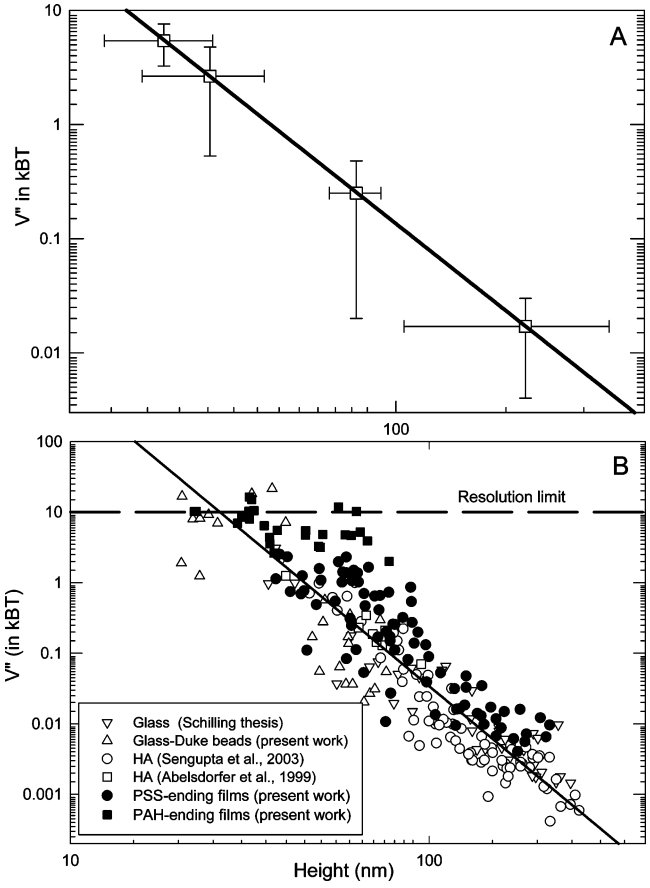


**Figure 10.** (A) Evolution of $V''$ as a function of the thickness of the PEI−(PSS/PAH)$_i$−PSS films as measured by DW−RICM. Each point represents the average of all the data (8−16 beads per film) obtained for films containing $i = 5$, 10, 20, and 30 layer pairs. The standard deviations (in $X$ and $Y$) are indicated by error bars. (B) Evolution of $V''$ as a function of the thickness obtained for different types of samples and surfaces: (▽) beads on glass (Schilling thesis); (△) Duke beads on glass (present work); (○) beads on a hyaluronic acid cushion (data from ref 27); (□) beads on a hyaluronic acid cushion (data from ref 28); (●) Duke beads on PSS-ending films (present work); and (■) Duke beads on PAH-ending films (present work).

effect probably results because the film is attached to an underlying hard substrate.

The second derivative of the interaction potential $V''$ can also be extracted from the autocorrelation function of the bead height fluctuations (see eq 3). In Figure 9B, $V''$ (for BSA-coated beads on PSS-ending films) is plotted as a function of the number of layer pairs in the PEM films. As can be seen, $V''$ decreases as the number of layer pairs increases. In Figure 10A, the $V''$ value and the height obtained for each given number $i$ of layer pairs (5, 10, 20, 30) have been gathered (same data as in Figure 9B) and the averages have been plotted. The monotonic decrease of $V''$, as a function of the height, can be fitted by the relation $V'' \approx h^{\alpha}$, with $\alpha = -4.33$.

This type of power law dependence also occurs in the case of ultrathin layers of hyaluronic acid[28] and for bare beads on bare glass. In all these cases, the exponent $\alpha$ is close to $-4$. To compare the present data with the data for beads on hyaluronic acid and bare glass, all the data have been gathered in Figure 10B. Note that two different types of beads were used for the experiments on hyaluronic acid and on bare glass: carboxyl-modified beads that were purchased from Duke Scientific (the same as in the present work) and carboxyl-modified PS beads that were purchased from Polysciences.

All the experimental data approximately follow the same power law (with $\alpha = 4.19$, $R = 0.84$, with $R$ being the linear regression coefficient). It thus seems that the stiffness of the potential experienced by a bead at a given height is determined solely by its height and not by any other parameter. Changing the ionic strength of the buffer or depositing polymer films between the bead and the glass substrate changes the equilibrium height of the bead and, hence, the stiffness of the potential. However, at a given equilibrium height, the beads always experience the same potential. Note that the working ionic strengths considered here are rather large (in the range of a few millimolar to a few hundred millimolar), whereas most studies of colloidal beads are conducted at much lower ionic strengths.[24,41] Our observations seem to indicate that, at high ionic strengths, the dominant contribution to the interaction potential comes from the glass surface itself and the intervening polymer layers do not have any significant role in determining the stiffness of this potential. The origin of this power law dependence is not clear and, until this issue is resolved, the elastic parameters extracted for relatively thin films from any colloidal probe technique will remain suspect.

## Discussion

In this work, DW−RICM was used to probe the structure and surface properties of PSS/PAH polyelectrolyte multilayer films, using colloidal probes, with special attention to surface properties of the probe beads. It was found that the surface of the carboxyl-modified beads, which were subsequently used as probes on the PSS/PAH films, is not hard but is comprised of an ∼10-nm-thick fuzzy polymer layer. Taking into account this fuzzy layer, the theoretically estimated heights for beads on bare glass were shown to agree well with the experiments reported here. For the PSS/PAH films, the measured heights correlate well with the thickness of the films, as estimated from OWLS measurements. By coating the beads and depositing polycations (PAH) or polyanions (PSS) as the outermost layer of the film, it was found that the relative charges of the beads and the topmost layer have an important role in determining the bead behavior. When the two were oppositely charged, the beads sunk into the films and hardly fluctuated at all. When both the beads and the topmost layer were negatively charged, the beads fluctuated in a quadratic potential and exhibited heights that were comparable to the expected film thickness. The height fluctuations of the beads were analyzed to yield the bead/film interaction potential and the effective film viscosity. Both the effective film viscosity and the stiffness of the potential decreased as the film thickness increased. In case of the stiffness of the potential, a power law dependence on the height was observed and a comparison with studies of colloidal beads on bare glass substrates and on hyaluronic acid cushions[27,28] showed that this power law dependence is universal with a common exponent.

**Acknowledgment.** We thank Guillaume Marzoff for its technical help in the zeta potential measurements and J. Crocker for helpful discussions about surfaces of PS beads. C.P. is grateful to the INSERM and the Deutsche Forschungsgemeinschaft (DFG) for financial support through a research visit fellowship at the E22 Laboratory (GZ: 418 FRA 112/2/03). G.M. is indebted to the Norwegian Research Council for financial support (Grant No. 134674/140). This work was supported by the Deutsche Forschungsgemeinschaft (SFB 563 B12) and by the Fonds der Chemischen Industrie.

## References and Notes


(1) Castner, D. G.; Ratner, B. D. *Surf. Sci.* **2002**, *500*, 28−60.
(2) Healy, K. E. *Curr. Opin. Solid State Mater. Sci.* **1999**, *4*, 381−387.
(3) Ratner, B. D.; Hoffman, A. S.; Schoen, F. J.; Lemons, J. E. *Biomaterials Science: An Introduction to Materials in Medicine*; Academic Press: New York, 1996.
(4) Decher, G.; Hong, J. D.; Schmitt, J. *Thin Solid Films* **1992**, *210*−*211*, 831−835.
(5) Decher, G. *Science* **1997**, *277*, 1232−1237.
(6) Bertrand, P.; Jonas, A.; Laschewsky, A.; Legras, R. *Macromol. Rapid Commun.* **2000**, *21*, 319−348.
(7) Dai, J.; Jensen, A.; Mohanty, D.; Erndt, J.; Bruening, M. *Langmuir* **2001**, *17*, 931−937.
(8) Hiller, J. A.; Mendelsohn, J. D.; Rubner, M. F. *Nature Mater.* **2002**, *1*, 59−63.
(9) Richert, L.; Lavalle, P.; Vautier, D.; Senger, B.; Stoltz, J.-F.; Schaaf, P.; Voegel, J.-C.; Picart, C. *Biomacromolecules* **2002**, *3*, 1170−1176.
(10) Mendelsohn, J. D.; Yang, S. Y.; Hiller, J.; Hochbaum, A. I.; Rubner, M. F. *Biomacromolecules* **2003**, *4*, 96−106.
(11) Caruso, F.; Niikura, K.; Furlong, D. N.; Okahata, Y. *Langmuir* **1997**, *13*, 3422−3426.
(12) Ruths, J.; Essler, F.; Decher, G.; Riegler, H. *Langmuir* **2000**, *16*, 8871−8878.
(13) Ladam, G.; Schaad, P.; Voegel, J.-C.; Schaaf, P.; Decher, G.; Cuisinier, F. G. *Langmuir* **2000**, *16*, 1249−1255.
(14) Ramsden, J. J.; Lvov, Y. M.; Decher, G. *Thin Solid Films* **1995**, *254*, 246−251.
(15) Picart, C.; Ladam, G.; Senger, B.; Voegel, J.-C.; Schaaf, P.; Cuisinier, F. J. G.; Gergely, C. *J. Chem. Phys.* **2001**, *115*, 1086−1094.
(16) Cunningham, B.; Lin, B.; Qiu, J.; Li, P.; Pepper, J.; Hugh, B. *Sens. Actuators B* **2002**, *85*, 219−226.
(17) Boura, C.; Menu, P.; Payan, E.; Picart, C.; Voegel, J.-C.; Muller, S.; Stoltz, J.-F. *Biomaterials* **2003**, *24*, 3521−3530.
(18) Tryoen-Toth, P.; Vautier, D.; Haikel, Y.; Voegel, J.-C.; Schaaf, P.; Chluba, J.; Ogier, J. *J. Biomed. Mater. Res.* **2002**, *60*, 657−667.
(19) Engler, A.; Bacakova, L.; Newman, C.; Hategan, A.; Griffin, M.; Discher, D. E. *Biophys. J.* **2004**, *86*, 617−628.
(20) Gao, C.; Donath, E.; Moya, S.; Dudnik, V.; Mohwald, H. *Eur. Phys. J. E* **2001**, *5*, 21−27.
(21) Dubreuil, F.; Elsner, N.; Fery, A. *Eur. Phys. J. E* **2003**, *12*, 215−221.
(22) Domke, J.; Radmacher, M. *Langmuir* **1998**, *14*, 3320−3325.
(23) Dimitriadis, E. K.; Horkay, F.; Maresca, J.; Kachar, B.; Chadwick, R. S. *Biophys J.* **2002**, *82*, 2798−2810.
(24) Bevan, M. A.; Prieve, D. C. *Langmuir* **1999**, *15*, 7925−7936.
(25) Behrens, S. H.; Plewa, J.; Grier, D. G. *Eur. Phys. J. E* **2003**, *10*, 115−121.
(26) Kühner, M.; Sackmann, E. *Langmuir* **1996**, *12*, 4866−4876.
(27) Albersdörfer, A.; Sackmann, E. *Eur. Biophys. J.* **1999**, *10*, 663−672.
(28) Sengupta, K.; Schilling, J.; Marx, S.; Fischer, M.; Bacher, A.; Sackmann, E. *Langmuir* **2003**, *19*, 1775−1781.
(29) Schilling, J.; Sengupta, K.; Goennenwein, S.; Bausch, A.; Sackmann, E. *Phys. Rev. E* **2003**, *68*.
(30) Wu, X.; van de Ven, T. G. M. *J. Colloid Interface Sci.* **1996**, *183*, 388−396.
(31) Raedler, J.; Sackmann, E. *Langmuir* **1992**, *8*, 848−853.
(32) Tiefenthaler, K.; Lukosz, W. *J. Opt. Soc. Am. B* **1989**, *6*, 209−220.
(33) Ramsden, J. J. *J. Mol. Recognit.* **1997**, *10*, 109−120.
(34) Picart, C.; Gergely, C.; Arntz, Y.; Schaaf, P.; Voegel, J.-C.; Cuisinier, F. J. G.; Senger, B. *Biosens. Bioelectron.* **2004**, in press.
(35) Zembala, M.; Déjardin, P. *Colloids Surf. B* **1994**, *3*, 119−129.
(36) Picart, C.; Lavalle, P.; Hubert, P.; Cuisinier, F. G.; Decher, G.; Schaaf, P.; Voegel, J.-C. *Langmuir* **2001**, *17*, 7414−7424.
(37) Gelbert, M.; Biesalski, M.; Ruhe, J.; Johannsmann, D. *Langmuir* **2000**, *16*, 5774−5784.
(38) Happel, J.; Brenner, H. *Low Reynolds Number Hydrodynamics*; Kluwer Academic Publishers: London, 1983.
(39) Israelachvili. *Intermolecular and Surface Forces*; Academic Press: London, 1992.
(40) Van de Ven, T. G. M. *Langmuir* **1996**, *12*, 5254−5262.
(41) von Grünberg, H. H.; Helden, L.; Leiderer, P.; Bechinger, C. *J. Chem. Phys.* **2001**, *114*, 10094−10104.
(42) Yoon, J. Y.; Park, H. Y.; Kim, J. H.; Kim, W. S. *J. Colloid Interface Sci.* **1996**, *177*, 613−620.
(43) Ladam, G.; Gergely, C.; Senger, B.; Decher, G.; Voegel, J.-C.; Schaaf, P.; Cuisinier. F. J. G *Biomacromolecules* **2000**, *1*, 674−688.
(44) Yoo, D.; Shiratori, S. S.; Rubner, M. F. *Macromolecules* **1998**, *31*, 4309−4318.
(45) Ladam, G.; Schaaf, P.; Cuisinier, F. G. J.; Decher, G.; Voegel, J.-C. *Langmuir* **2001**, *17*, 878−882.
(46) Brenner, H. *Chem. Eng. Sci.* **1961**, *16*, 242−251.